Spatially Resolved Surface Analysis of an Octadecanethiol Self-Assembled Monolayer on Mild Steel Using Sum Frequency Generation Imaging Microscopy

Katherine Cimatu and Steven Baldelli*

Department of Chemistry, University of Houston, Houston, Texas 77204

Received: January 5, 2007; In Final Form: March 15, 2007

Sum frequency generation imaging microscopy has been used to investigate a self-assembled monolayer of an alkanethiol (octadecanethiol, ODT) on a mild steel surface. The images are used to analyze the orientation of the alkanethiol monolayer and the distribution of orientational angles as well as defects in the film. The results show that, on average, ODT forms an ordered monolayer on mild steel when compared to the same monolayer on gold. However, the image analysis suggests that the distribution of tilt angles and conformational defects is greater for ODT on a mild steel surface compared to ODT/Au.

Introduction

A persistent problem in the analysis of solid surfaces is that even a carefully prepared surface contains defects in the range of 0.1−1000 μm.[1−4] These defects are, for example, from scratches, impregnated particles from polishing, or other foreign materials. The molecules adsorbed at or near these sites dramatically influence the surface properties in applications such as corrosion inhibition, catalysis, electronics, and biocompatibility.[5,6] As a result, analysis of the average surface properties is misleading when the spatial distribution of the molecules on the surface is not taken into account. Thus, surface characterization with spatial resolution has its benefits in obtaining structural and topological differences and also acquiring chemical information.[7,8]

The ability to spectroscopically and spatially investigate surfaces is not common in a single-probe technique because each method has its own limitation.[9] Sum frequency generation (SFG) imaging is able to address some of these issues since it has a high surface specificity, submonolayer sensitivity, chemical selectivity, and a potential spatial resolution of approximately 1 μm.[10−13] This study focuses on the utilization of this imaging technique to determine the chemical composition of an alkanethiolate monolayer at the gas−metal interface and differentiate the molecules oriented at a local region versus the sample average. Spatial resolution is achieved without scanning and focusing on the sample but rather using collimated input beams and having the SFG signal imaged onto a CCD camera. Self-assembled monolayers (SAMs) on metal surfaces provide a good model system to demonstrate the significance of a heterogeneous surface film.

A two-dimensional surface analysis of octadecanethiol (ODT) on mild steel (MS) is performed using sum frequency generation imaging microscopy (SFGIM). A systematic statistical analysis of SFG spectra at different surface positions is performed to obtain the symmetric and antisymmetric ratios of the CH_3 stretches (CH_3 sym/asym) to provide the distribution of tilt angles for the terminal methyl group. In addition, the CH_2/CH_3 (sym) ratio is obtained to estimate the degree of conformational disorder of the alkyl chain in the monolayer. SFG imaging microscopy is able to deduce tilt angle and defect distributions of the ODT molecules across the mild steel surface. In summary, ODT−MS has a wider range of tilt angles and conformational disorder but is still considered a well-ordered monolayer when compared to the ODT−Au system.

Background

SFG is a second-order surface-sensitive nonlinear process,[14] and as a surface technique, SFG spectroscopy has become a very effective tool in obtaining the vibrational spectra of molecules at the interface.[15] In general, the SFG process involves the spatial and temporal overlap of two pulsed laser beams on the surface with molecules in a noncentrosymmetric environment to generate the SFG signal effectively.[14−16] The generation process is proportional to the second-order nonlinear susceptibility, $\chi^{(2)}$, which contains the vibrational molecular information, $\chi_R^{(2)}$, and a nonresonant term, $\chi_{NR}^{(2)}$, shown as

$$\chi^{(2)} = \chi_{NR}^{(2)} + \chi_R^{(2)} = \chi_{NR}^{(2)} + \sum_q \frac{N\langle\beta^{(2)}\rangle}{\omega_{IR} - \omega_q + i\Gamma} \qquad (1)$$

where N is the total number of vibrational modes and $\langle\beta^2\rangle$ is the orientational averaged hyperpolarizability, which contains the IR and Raman transition moments. Accordingly, as the IR laser frequency, ω_{IR}, approaches the qth vibrational mode, ω_q, of the molecules at the interface, resonance enhancement of the SFG intensity is observed. Plotting the SFG intensity as a function of the IR wavenumber yields a vibrational spectrum which has either a peak or a dip. The peak or dip is a result of the interference between $\chi_R^{(2)}$ and $\chi_{NR}^{(2)}$ that is either constructive or destructive interference depending on the phase and magnitude of the terms, respectively.[17−20]

Experimental Section

The sample was prepared by purchasing the standard reagents (ODT, $CH_3(CH_2)_{17}SH$, 98%; LiCl, anhydrous, 99% minimum; MeOH, 99.9%, spectrophotometric grade) and using them as received. The mild steel electrode from Champion Technologies was mounted onto a Teflon sheath. The electrode was polished down to 0.05 μm with alumina slurry and then sonicated with ethanol to remove the polishing residues. It was then rinsed with water and methanol. Next the electrode was placed in a three-electrode electrochemical cell with a 0.1 M $LiCl/CH_3OH$

10.1021/jp070095s CCC: $37.00
Published on Web 04/21/2007

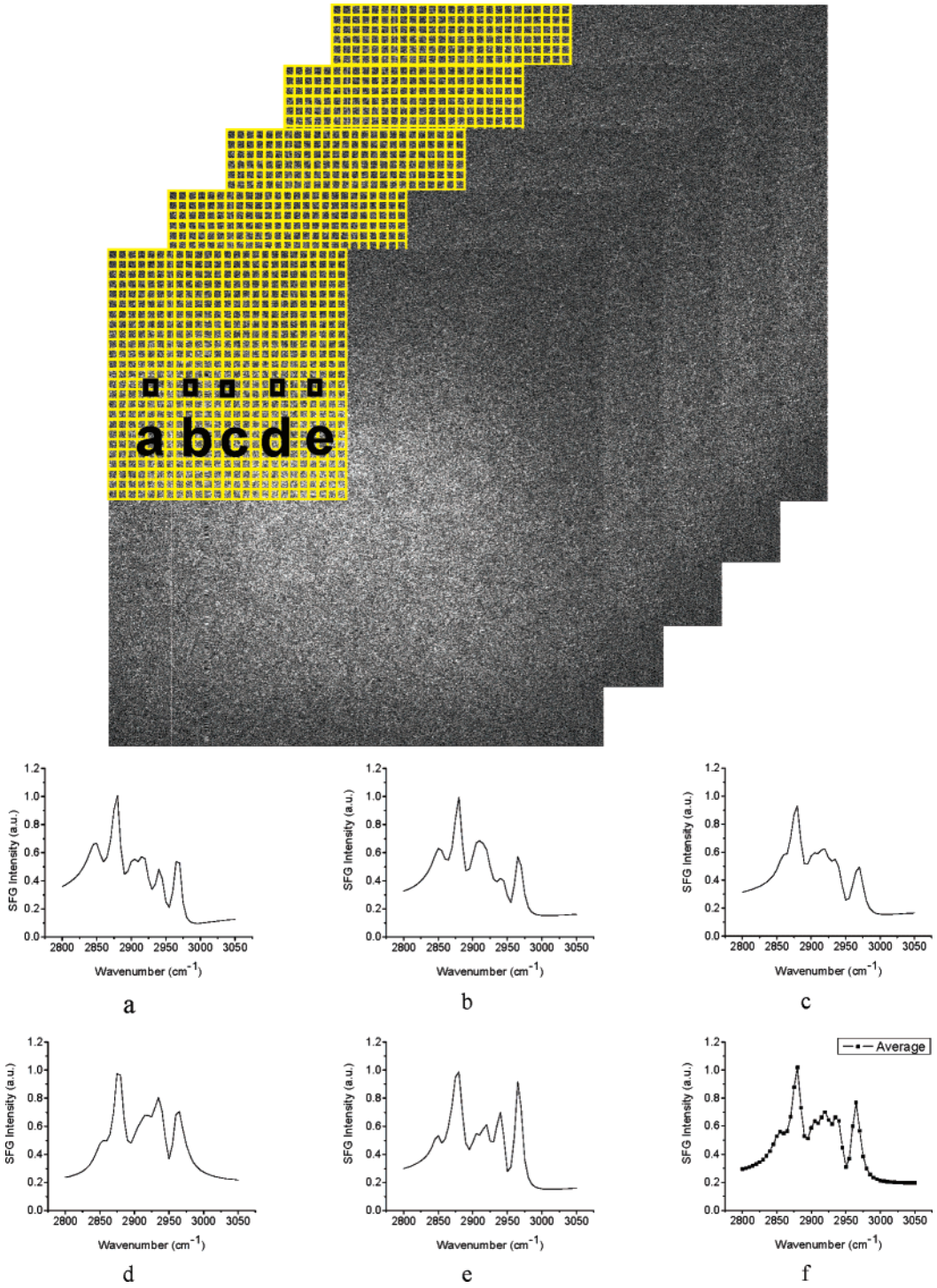

Figure 1. An example of a stack of images partitioned into a 20 × 20 pixel area (white squares) where the small black squares represent areas of positions a−e: (a−e) spectra of the five black square regions labeled from a to e from the stack; (f) average spectrum of the entire area (nonimaging).

solution purged with N_2(g). A reducing potential of −1.2 V was applied for 20 min, at which point ∼1 mmol of ODT was injected into the solution. After 2 h, the potentiometer was switched off, and the MS electrode was taken out of the solution. The MS electrode was rinsed with methanol and dried under a stream of N_2 gas.[21] On the basis of the previous results, as stated by Zhang and Baldelli, the alkanethiol molecules self-assembled with applied potential on MS that forms a well-ordered monolayer on the basis of the interpretation of the average SFG spectra and electrochemical measurements.[21] After sample preparation, the sample was aligned in the SFG microscope.[10,22]

The laser system consists of a pulsed picosecond Nd:YAG laser (model PL2143A/20 from Ekspla) used to generate the fundamental 1064 nm beam that pumps the optical parametric generator/amplifier (OPG/OPA). The OPG/OPA generates the tunable infrared (IR) beam from 2000 to 4000 cm^{-1}. Both beams, as used in the experiments, have a pulse duration of ∼20 ps and a repetition rate of 20 Hz.

The SFG microscope was constructed using a reflection configuration. The 1064 nm and the tunable IR beams are both set to p-polarization. There was no polarizer set at the output for the SFG beam. The two collimated incident beams which are set at angles of 70.0° (IR) and 60.0° (1064 nm) are spatially

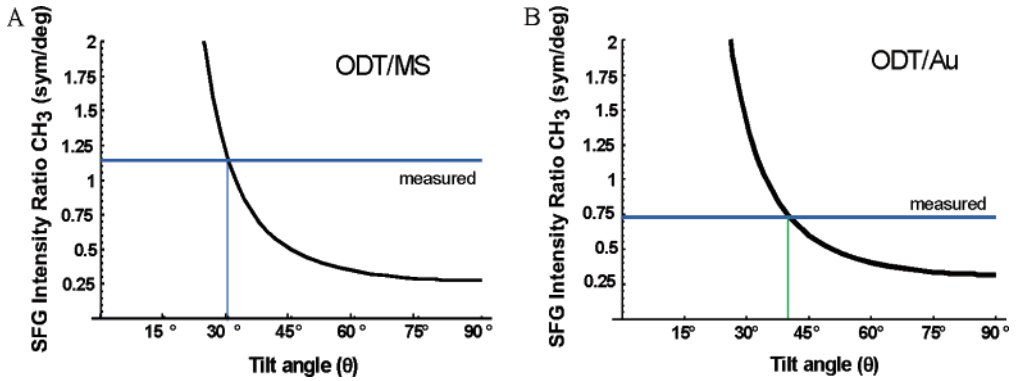

Figure 2. Orientation analysis of the average SFG using δ function analysis for ODT on (A) mild steel and (B) gold. Measured values shown are representative, corresponding to various bins in the histogram (Figures 4 and 5).

and temporally overlapped at the interface to generate a coherent SFG beam at an exact angle from 62.0° to 62.3°.

This coherent and collimated (maintained by relevant optics in the system) SFG signal was detected spatially by imaging onto the CCD camera.[2,10,13,22] Before the signal was imaged onto the CCD, a set of two lenses acted as a telescope to maintain the 1:1 image ratio of the SFG beam. This SFG beam was then diffracted by the diffraction grating (600 grooves/mm) perpendicularly onto the objective with 10× magnification. A tube lens was placed after the objective to maintain the collimation of the SFG beam before it was imaged onto the CCD camera (Roper Scientific). The spatial resolution of the microscope is approximately 10 μm using the Air Force pattern as a standard that provided 10 μm stripes to test the resolution. The resolution was determined using the Rayleigh criterion.[22]

SFG images and spectra were obtained by scanning the IR from 2800 to 3050 cm^{-1} at 0.02 cm^{-1}/s, which corresponds to one image per 5 cm^{-1} (5000 laser shots). Using the Winspec software, the images were acquired every 4 min and 6 s, which is equivalent to 5000 accumulations, while the infrared was continuously scanned at a rate of 0.02 cm^{-1}/s.

Figure 1f shows the reference spectrum of the ODT−MS taken using the nonimaging SFG spectroscopy to specify the assignment of the peaks. The assigned peaks are the following: 2875, 2938, and 2967 cm^{-1}, which correspond to the terminal methyl (CH_3) symmetric stretch, Fermi resonance, and CH_3 antisymmetric stretch, respectively. The other weak vibrational stretches present in the spectrum at 2850 and 2915 cm^{-1} are the methylene (CH_2) symmetric and antisymmetric vibrational modes, presumably due to gauche defects in the alkyl chains. There are two additional peaks present in the SFGIM ODT−MS spectrum which are the Fermi resonance CH_2 symmetric stretch at 2904 cm^{-1} and the out-of-plane CH_3 antisymmetric stretch (dip) at 2955 cm^{-1}, respectively.[23−25]

As shown in Figure 1, the postanalysis was accomplished by stacking all the images from 2800 to 3050 cm^{-1}, where the 51 images were processed by extracting the intensities from each region of interest (ROI) and plotted as a function of the IR wavenumber using ImageJ and Origin 6.0 software. The image analysis for the local region was performed using 20 × 20 pixel areas over the entire 1024 × 1024 pixel area of the CCD, which has a total of 2621 regions, Figure 1. The partitioning of one whole image to 20 × 20 pixel areas starts from left to right and from top to bottom (designated pixels 0−20 up to pixels 1000−1024). These specific areas were the so-called ROIs, which means that each of these areas have the corresponding intensities (normalized) that were plotted as a function of the IR frequency. As an example, local spectra for five representative areas are presented in Figure 1a−e. After

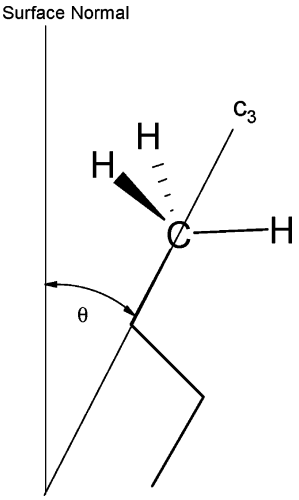

Figure 3. Geometry of the terminal methyl group at the end of a trans-extended alkane chain.

plotting, the spectra were fitted using eq 1 to obtain the amplitude, frequency, and width of each peak. The corresponding data from the fittings were used in obtaining the SFG intensity ratios for further analysis of the orientation of the thiol molecules on the substrate. As a reference sample, ODT on Au was prepared by using standard methods.[15,26,27] A 1 mM solution of octadecanethiol was prepared in ethanol solution. Gold surfaces were immersed in the solution for the self-assembly for up to 18 h. The same analysis was performed on the SFG imaging data of ODT on Au.

Results and Discussion

Each ROI is analyzed on the basis of Figure 1 (spatially, 2621 regions) to develop the ensemble of the entire area. This is the experimentally determined distribution of the molecules where the number of occurrences (i.e., counts) of the ratio is plotted as a histogram and fit to a Gaussian distribution function to obtain the average and standard deviation. These ratios are the input used in the SFG analysis (Figure 2) to explicitly account for the spread in tilt angles of CH_3 groups on the surface. Further, the tilt angle determined from the SFG analysis is mapped back onto the surface to visualize the sample's spatial heterogeneity, Figure 4A.

SFG spectral data are transformed into orientation analysis by taking ratios of the peak intensities derived from curve fitting analysis. In this analysis, the ratio between the symmetric (sym) and antisymmetric (asym) vibrations of the terminal methyl group is used to deduce the orientation.[28−32] The intensity ratio for CH_3 (sym/asym) is plotted vs the tilt angle (θ) of the C_3

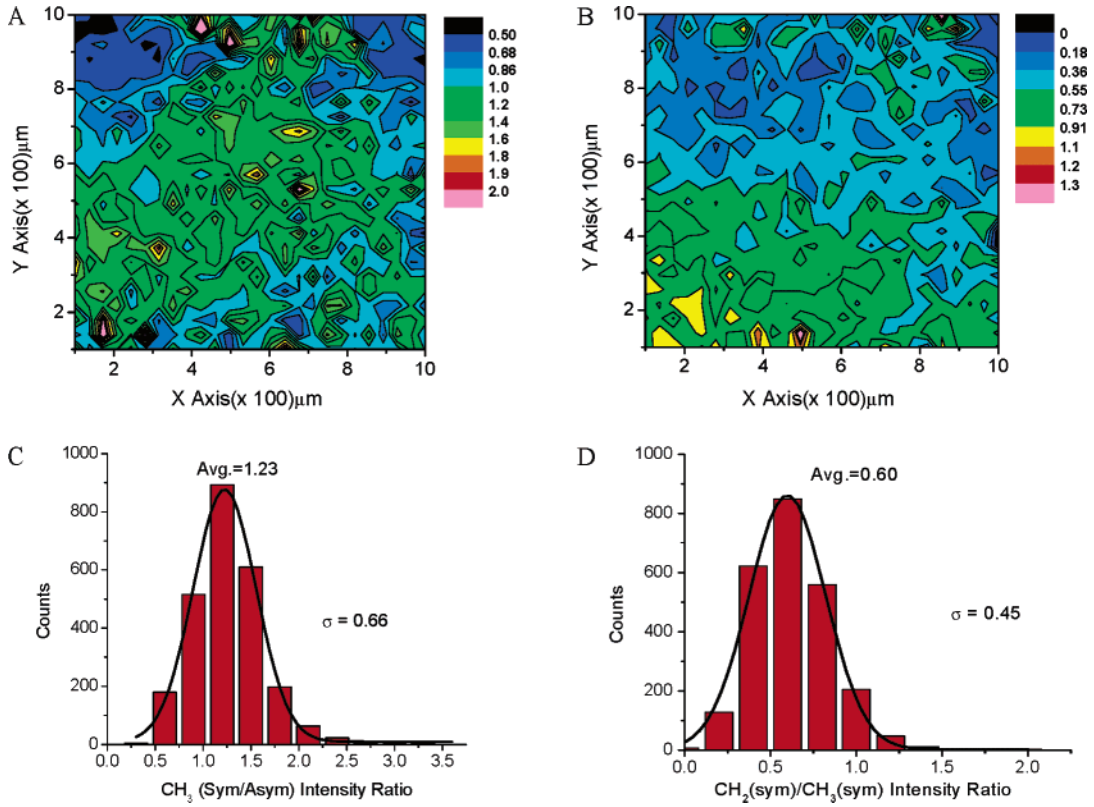

Figure 4. SFG imaging analysis for ODT/MS. Contour plots of (A) CH_3 (sym/asym) intensity ratios (scale is atomic units) and (B) CH_2/CH_3 (sym) intensity ratios. (C, D) Histogram plots of the same ratios, respectively.

axis from the surface normal in Figure 2, where this analysis uses the δ function distribution (i.e., all molecules have identical angles). Each ROI is considered to have a δ function distribution.

Parts A and B of Figure 4 show the spatial distribution (map) of the (A) CH_3 (sym/asym) ratio for tilt angle interpretation and (B) CH_2/CH_3 (sym) ratio for the number of defects (local distribution of defects across the area) represented by the contour plot.

Analysis of the SFG images for ODT on MS is compared to the well-established information available for ODT on gold.[27] Insight into the structure of the ODT monolayer is obtained from the SFG imaging analysis.

First, SFG spectra are used to deduce the average tilt angle from CH_3 the (sym/asym) ratio.[29,31,32] Under nonimaging conditions, this analysis provides the so-called δ function orientation where all groups are considered to have a single tilt angle (θ). This is not a physically reasonable situation. However, using spatially resolved SFG spectra, each ROI becomes one component of the entire ensemble, and therefore, the distribution is directly determined. The size for the specific regions of interest in this experiment is 20×20 μm^2.

Tilt Angle Analysis. The histogram plots of CH_3 (sym/asym) for ODT on MS and Au are presented in Figures 4C and 5C, respectively. From this analysis, two important observations are made. First, the average values are different, i.e., different tilt angles on the two surfaces. On Au, the ratio is 0.87, which corresponds to a tilt angle of 37° from the surface normal. On MS, the ratio is 1.23 and is consistent with a tilt angle of 29°. Then the calculated intensity ratios are mapped back onto the surface to observe the surface's heterogeneity (on the basis of the difference in color which pertains to the intensity ratio at a specific area), Figures 4A and 5A. It is interesting to note that without consideration of the distribution (nonimaging SFG) the tilt angles are determined to be 30° and 23° for ODT/Au and ODT/MS, respectively.[21] Second, each system has a different distribution width for the tilt angle. The width, from the Gaussian curve, is a measure of the degree of surface heterogeneity. The CH_3 (sym/asym) ratio for each ROI is summarized in the histograms shown in Figures 4C and 5C and also transformed into a tilt orientation as given in Figure 2A. Thus, the results show tilt angle ranges of about 9° for ODT/Au and 17° for ODT/MS. The interpretation is that the surface monolayer is less oriented on MS than Au. Important information is neglected or overlooked that leads to a misinterpretation of the degree of homogeneity for SAMs on the metal surface when only the average spectrum is considered.

Film Disorder Analysis. SFG spectra are also useful in determining how densely packed (or "perfect") the chains in the film are by considering the conformational defects. It is suggested that, as the alkyl chain deviates from the all-trans configuration, pairs of CH_2 groups without an inversion center will appear in the SFG spectrum.[15,26,33,34] Since an ideally dense monolayer, theoretically, has no conformational defects, the CH_2/CH_3 (sym) stretching ratio is commonly used as a guide to determine the degree of disorder in the monolayer.[35] The 1-alkanethiols on gold are considered the standard of a well-ordered monolayer; thus, this system is used to compare with the ODT on MS.

In considering conformational defects across the surface, the ratios of the CH_2/CH_3 (sym) intensities are obtained from spectral analysis. These ratios are compared in the histograms shown in Figure 4D for ODT on MS and Figure 5D for ODT on Au. The CH_2/CH_3 (sym) ratio for ODT/Au is $\sim$0.04, while on MS this ratio is 0.6. The average values clearly demonstrate that as the ratio deviates from zero the monolayer contains more defects on MS than on Au. The ratios of these two surfaces are

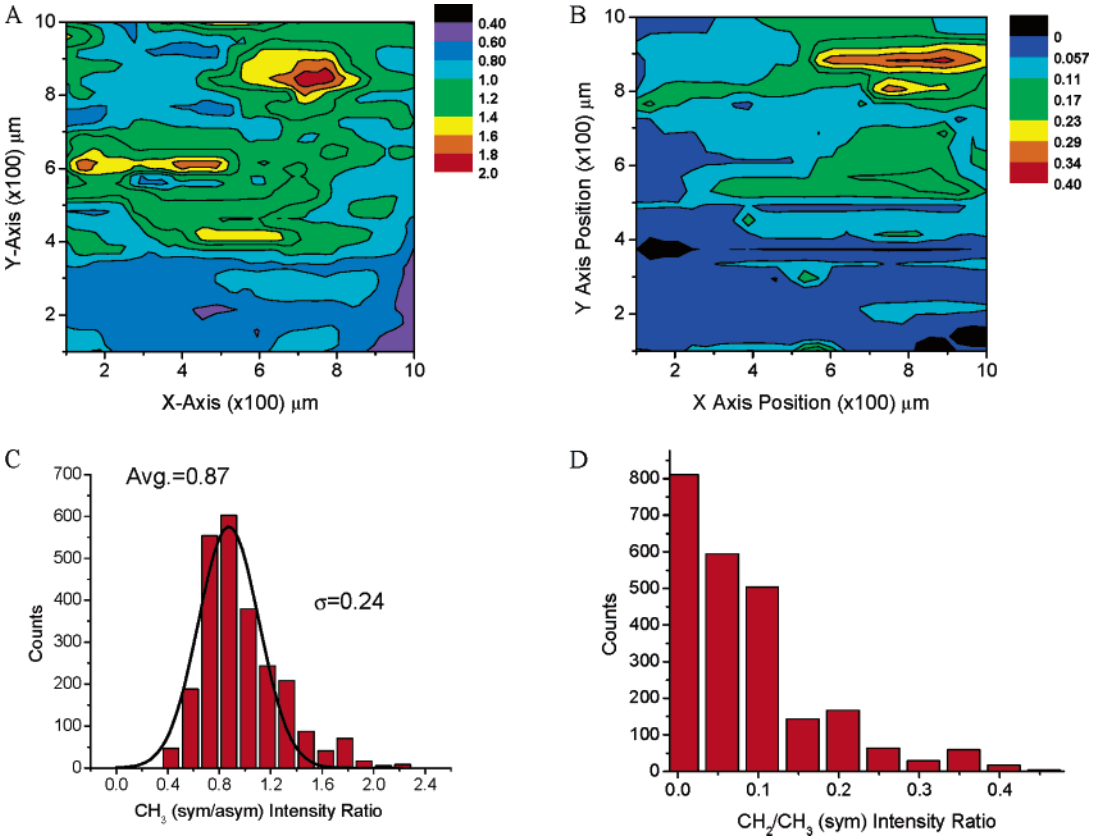

Figure 5. SFG imaging analysis for ODT/Au. Contour plots of (A) CH_3 (sym/asym) intensity ratios and (B) CH_2/CH_3 (sym) intensity ratios. (C, D) Histogram plots of the same ratios, respectively.

also mapped to spatially visualize surface heterogeneity of ODT/MS compared to ODT/Au in Figures 4B and Figure 5B.

Interpretation. Imaging improves the interpretation and understanding of surface chemistry by selecting and analyzing each region separately. Using nonimaging SFG spectra, it is only the oriented part of the surface which clearly gives a signal. Therefore, in an average SFG, the more well oriented regions dominate the spectrum compared to the less oriented domains of the surface. Thus, relying only on the average analysis results in losing important information of the monolayer on metal surfaces.

It is not too surprising that SAMs on MS are less ideal than on Au due to the nature of the substrate since mild steel is a reactive metal under ambient laboratory conditions. The maps shown (Figure 4) depict the inhomogeneity of the surface monolayer, which is due to a number of reasons: (1) substrate/metal property (impurities); (2) sample preparation; (3) defects on the mild steel electrode before the formation of the ODT monolayer; (4) formation of the oxide layer that inhibits the ability of alkanethiols to self-assemble. This is verified by the preparation condition where it was shown that ODT does not assemble onto an oxidized MS surface since the formation of a metal−sulfur bond is critical to monolayer formation.[21] Therefore, ODT molecules assembled on (or near) defect sites are less well ordered with respect to the orientation and conformation of the molecules. On the other hand, the situation on Au is significantly different, since Au does not form a stable oxide at room temperature and remains metallic. Further, a well-prepared surface has minimal defects, and since Au is a pure element, it does not have significant impurities. These factors allow the assembly process to occur and the ODT molecules to form a more dense monolayer.

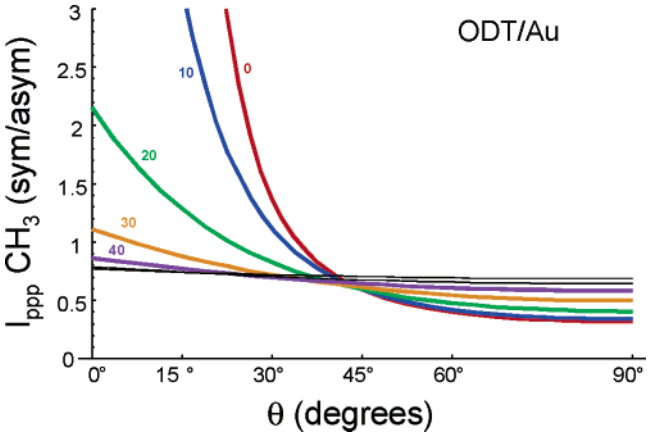

Figure 6. SFG intensity ratio CH_3 sym/asym vs tilt angle. Each curve represents a different distribution width (σ, deg) where $\sigma = 0°$ is a δ function distribution (red curve).

Although the ODT/Au system is very well ordered, there are still some areas of ODT molecules that are less ordered, and these sites are also considered to be important to the overall performance of the film. On MS, the film as a whole is also still considered to be a well-oriented monolayer; however, there is a significant amount of defects that are presumed to be responsible for the limited corrosion protection that the ODT SAM provides to MS.[21] This point is not obvious from using the average SFG analysis but is clear from the standpoint of SFG imaging microscopy. Furthermore, the individual spatial region provides the statistical treatment of the monolayer on the basis of obtaining the SFG spectra at each specific region

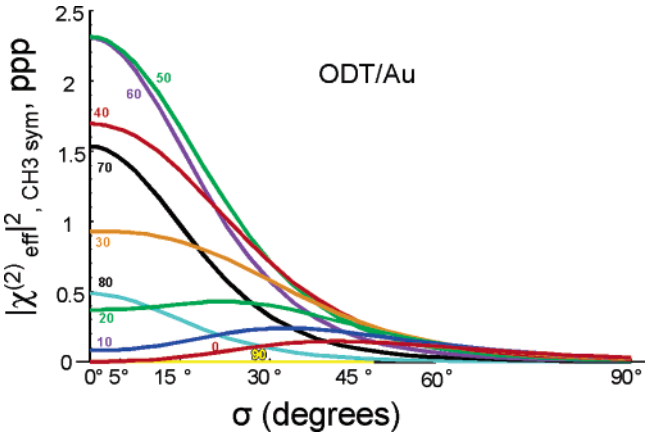

Figure 7. $|\chi^{(2)}|^2$ vs σ. Each curve represents a different average tilt angle from the surface normal, θ. The red curve at 0° is along the surface normal.

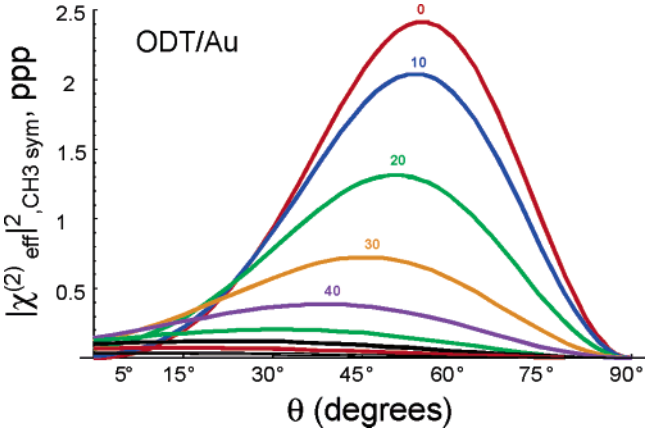

Figure 8. $|\chi^{(2)}|^2$ vs θ. Each curve represent a different distribution width (deg). $\sigma = 0°$ is a δ function distribution.

and then providing the ensemble average of the thiol molecules at the metal surface.

Measurements of the average SFG surface signal do not provide a unique orientation angle considering that each monolayer has its own distribution of tilt angles. For example, consider Figure 6, which presents the calculated SFG intensity ratio of the terminal methyl group (CH_3 sym/asym) versus the tilt angle from the surface normal, θ. Each curve in Figure 6 assumes a different distribution width and range of tilt angles based on the Gaussian distribution function. $\sigma = 0°$ is the δ function distribution, which states that all methyl groups are at the same tilt angle. This is a physically unreasonable state. Therefore, in this situation, assuming a distribution of angles around a mean (average) is considered, this distribution is typically the Gaussian distribution, although there is no physical justification for this.[36] The other curves (Figure 6) represent increasing distribution widths, $\sigma = 10°$, 20°, 30°, etc. Thus, in considering the measured CH_3 sym/asym ratio as 1.25, in the case of ODT/Au, the data presented are consistent with tilt angles/distribution width pairs: (30°, $\sigma = 0°$), (27°, $\sigma = 10°$), (15°, $\sigma = 20°$), or, (0°, $\sigma = 28°$). From the measurement provided, exact tilt angle orientation and distribution width values are not uniquely determined. One advantage of sum frequency imaging is the ability to experimentally determine the distribution and obtain a more accurate view of the surface. Another significant aspect demonstrated in Figure 6 is that, as the distribution width becomes larger than $\sigma > 40°$ (±20°), SFG has a limitation of not being able to determine the orientation angle at the surface since the data are more consistent with a larger range of orientations. As the surface becomes more random, SFG is less sensitive. This point is also demonstrated in Figure 7 (for the ODT/Au system), which has the plots of the square of the effective susceptibility for CH_3 sym vs the distribution width (deg). The SFG signal intensity is proportional to $|\chi^{(2)}|^2$, and the degree of orientation is related to the distribution width, σ. Therefore, Figure 7 is interpreted as SFG signal intensity vs orientation. Again, as the distribution broadens, the SFG signal is observed to drop dramatically. This is consistent with the description that SFG signal is approximately zero in an isotropic medium.

This result has important implications for the interpretation of the SFG signal from a spatially heterogeneous surface. It suggests that, in regions where molecules have a broader distribution, the contribution to the average SFG signal is much less than in those regions where the distribution is narrow. Even a small change in the distribution substantially changes the SFG signal intensity. However, SFG imaging allows the regions with less SFG signal to be regarded equally since each region is measured independently as discussed. That is, by obtaining the ensemble average from the 1024 × 1024 pixel area for a total of 2621 specific areas, these regions that have a lower signal are properly accounted for in the orientation analysis. Even though these regions have a lower SFG signal, these specific areas may actually have a larger coverage on the surface and may be more important to the overall surface chemistry.

Another related effect is demonstrated in Figures 7 and 8. Certain tilt angle orientations contribute to the SFG intensity more than others. Each curve in Figure 7 is for a different average tilt angle orientation, which shows that for a given σ the SFG intensity as a function of the tilt angle varies in a nonlinear way (see also Figure 8). In Figure 7, this plot shows that tilt orientations near 50−60° contribute more (25×) to the SFG signal while those from 0° to 20° or from 80° to 90° contribute much less. This suggests that SFG analysis of the average favors those at 50−60°; thus, much of the SFG orientation analysis in the literature tends toward the magic angle value of 60°.

Another perspective of this effect is shown in Figure 8, where for narrow distributions, <20°, the SFG signal is larger near tilt angles of 50−60°. This is similar to the magic angle results of SHG for molecules on a rough surface as presented by Simpson and Rowlen.[37,38] The difference in SFG signal intensity is less if the distribution is broad, but then not much is known about the average orientation and range at this point. Again, SFG imaging and the subsequent analysis are able to deduce the distribution experimentally to provide the local structure and a more meaningful interpretation of the surface orientation.

Conclusion

SFG imaging allows the visualization of the surface structure and relates the local structure to the overall performance of the material. For example, it is known that the wetting properties, friction, and especially corrosion inhibition of SAMs are influenced by the degree of order in the film. These properties are usually measured over a size scale of millimeters. Therefore, the use of imaging spectroscopy to evaluate the quality and structure of monolayer films is useful to understand local wetting and frictional properties or deviations from the average measurements. SFG imaging microscopy has been used to characterize a monolayer of ODT on Au and MS and has demonstrated that the monolayer on the reactive metal surface (MS) is less well ordered compared to that on Au.

Acknowledgment. We thank Research Corp., GEAR, and Champion Technologies (Houston, TX) for support of this work. Thanks are also due to John Glenn Ramon and Amy Hazelrigg of the University of Houston for software development.

References and Notes

(1) Committee on Revealing Chemistry through Advanced Chemical Imaging, N. R. C. *Visualizing Chemistry: The Progress and Promise of Advanced Chemical Imaging*; National Academies Press: Washington, DC, 2006.

(2) Kuhnke, K.; Hoffmann, D. M.; Wu, X. C.; Bittner, A. M.; Kern, K. *Appl. Phys Lett.* **2003**, *83*, 3830.

(3) Zumbusch, A.; Holtom, G. R.; Xie, X. S. *Phys. Rev. Lett.* **1999**, *82*, 4142.

(4) Eiswirth, M.; Ertl, G. In *Chemical Waves and Patterns*; Kapral, R., Showalter, K., Eds.; Kluwer Academic Publishers: Boston, 1995; p 447.

(5) Engel, W.; Kordesch, M. E.; Rotermund, H. H.; Kubala, S.; von Oetzen, A. *Ultramicroscopy* **1991**, *36*, 148.

(6) Jones, D. *Principles and Prevention of Corrosion*, 2nd ed.; Prentice Hall: Upper Saddle River, NJ, 1996.

(7) Akhremitchev, B. B.; Pollack, S.; Walker, G. C. *Langmuir* **2001**, *17*, 2774.

(8) Akhremitchev, B. B.; Sun, Y.; Stebounova, L.; Walker, G. C. *Langmuir* **2002**, *18*, 5325.

(9) Lipkowski, J., Ross, P. N., Eds. *Imaging of Surfaces and Intefaces*; Wiley-VCH: New York, 1999.

(10) Cimatu, K. A.; Baldelli, S. *J. Phys. Chem. B* **2006**, *110*, 1807.

(11) Hoffmann, D. M.; Kuhnke, K.; Kern, K. *Rev. Sci. Instrum.* **2002**, *73*, 3221.

(12) Florsheimer, M.; Brillert, C.; Fuchs, H. *Langmuir* **1999**, *15*, 5437.

(13) Florsheimer, M.; Brillert, C.; Fuchs, H. *Mater. Sci. Eng., C* **1999**, *8*−*9*, 335.

(14) Guyot-Sionnest, P.; Tadjeddine, A. *Chem. Phys. Lett.* **1990**, *172*, 341.

(15) Bain, C. D. *J. Chem. Soc., Faraday Trans.* **1995**, *91*, 1281.

(16) Bain, C. D.; Davies, P. B.; Ong, T. H.; Ward, R. N. *Langmuir* **1991**, *7*, 1563.

(17) Duffy, D. C.; Davies, P. B.; Creeth, A. M. *Langmuir* **1995**, *11*, 2931.

(18) Ward, R.; Duffy, D. C.; Davies, P. B. *J. Phys. Chem.* **1994**, *98*, 8536.

(19) Ward, R. N.; Davies, P. B.; Bain, C. D. *J. Phys. Chem.* **1993**, *97*, 7141.

(20) Florsheimer, M.; Bosch, M.; Brillert, C.; Wierschem, M.; Fuchs, H. *J. Vac. Sci. Technol., B* **1997**, *15*, 1564.

(21) Zhang, H. P.; Romero, C. R.; Baldelli, S. *J. Phys. Chem. B* **2005**, *109*, 15520.

(22) Cimatu, K. A.; Baldelli, S. *J. Am. Chem. Soc.* **2006**, *128*, 16016.

(23) Snyder, R. G. *J. Chem. Phys.* **1965**, *42*, 1744.

(24) Snyder, R. G.; Strauss, H. L.; Elliger, C. A. *J. Phys. Chem.* **1982**, *86*, 5145.

(25) MacPhail, R. A.; Strauss, H. L.; Snyder, R. G.; Elliger, C. A. *J. Phys. Chem.* **1984**, *88*, 334.

(26) Potterton, E. A.; Bain, C. D. *J. Electroanal. Chem.* **1996**, *409*, 109.

(27) Love, J. C.; Estroff, L. A.; Kriebel, J. K.; Nuzzo, R. G.; Whitesides, G. M. *Chem. Rev.* **2005**, *105*, 1103.

(28) Lu, R.; Gan, W.; Wu, B. H.; Zhang, Z.; Guo, Y.; Wang, H. F. *J. Phys. Chem. B* **2005**, *109*, 14118.

(29) Wang, H. F.; Gan, W.; Lu, R.; Rao, Y.; Wu, B. H. *Int. Rev. Phys. Chem.* **2005**, *24*, 191.

(30) Huang, J. Y.; Shen, Y. R. In *Laser Spectroscopy and Photochemistry on Metal Surfaces*; Dai, H. L., Ho, W., Eds.; World Scientific: Singapore, 1995.

(31) Hirose, C.; Yamamoto, H.; Akamatsu, N.; Domen, K. *J. Phys. Chem.* **1993**, *97*, 10064.

(32) Hirose, C.; Akamatsu, N.; Domen, K. *J. Chem. Phys.* **1992**, *96*, 997.

(33) Ward, R. N.; Davies, P. B.; Bain, C. D. *J. Phys. Chem. B* **1997**, *101*, 1594.

(34) Miranda, P. B.; Shen, Y. R. *J. Phys. Chem. B* **1999**, *103*, 3292.

(35) Hunt, J. H.; Guyot-Sionnest, P.; Shen, Y. R. *Chem. Phys. Lett.* **1987**, *133*, 189.

(36) Wang, J.; Paszti, Z.; Even, M. A.; Chen, Z. *J. Am. Chem. Soc.* **2002**, *124*, 7016.

(37) Simpson, G. J.; Rowlen, K. L. *J. Am. Chem. Soc.* **1999**, *121*, 2635.

(38) Simpson, G. J.; Rowlen, K. L. *J. Phys. Chem. B* **1999**, *103*, 1525.